IV International Conference on Computational Methods for Coupled Problems in Science and Engineering
COUPLED PROBLEMS 2011
M. Papadrakakis, E. Oñate and B. Schrefler (Eds)

MAGNETIZATION MODELS FOR PARTICLE-BASED SIMULATIONS OF MAGNETORHEOLOGICAL FLUIDS

HANNA G. LAGGER*, JOËL PEGUIRON*, CLAAS BIERWISCH* AND MICHAEL MOSELER*

* Fraunhofer Institute for Mechanics of Materials IWM
Wöhlerstrasse 11, 79108 Freiburg, Germany
e-mail: hanna.lagger@iwm.fraunhofer.de, www.iwm.fraunhofer.de

Key words: Magnetorheological Fluid, Magnetization Model, Discrete Element Method, Numerical Simulation

Abstract. In this study, three-dimensional particle-based simulations are used to model magnetorheological fluids. The numerical model of the MRF is implemented in the framework of the Discrete Element Method (DEM) and takes into account the coupling of the magnetic dipoles, the hydrodynamic drag forces and steric forces between particles. To accurately treat the magnetic interaction between particles, the magnetic field at the particles' position is computed and an appropriate magnetization model is implemented. DEM simulations with different volume fractions of the MRF are carried out and the resulting magnetization curves are put in comparison with experimental data.

1 INTRODUCTION

Typical magnetorheological fluids (MRF) consist of magnetically permeable particles (e.g. iron) in carrier oil. Upon activation of an external magnetic field, the apparent viscosity of the MRF changes within a few milliseconds by orders of magnitude, inducing a change of the MRF from liquid to solid. By controlling the strength of the magnetic field, the viscosity of the MRF can be adjusted very accurately. For this reason, MRF are highly interesting for several industrial applications, such as controllable dampers or automotive clutches.

In this work we use numerical simulations to investigate the mechanisms which govern the behaviour of the MRF when subjected to a magnetic field. Inside the MRF, the contribution of the magnetized particles to the local magnetic field cannot be neglected [1]. Therefore an accurate description of the particles' magnetization is required. We can experimentally assess magnetization curves of magnetorheological fluids, but not of single particles. Different magnetization functions to model the response of an iron particle to a magnetic field can be found in the literature [2, 3, 4], however there is no well-established

magnetization function which is suitable for every MRF. A specific magnetization function is an arbitrary choice and can also be different for different materials [5]. Here we choose to perform simulations based on different single-particle magnetization functions, compare the resulting MRF magnetization curves to experiments [4, 6] and adapt the curve parameters.

In Sec. 2 the simulation method is presented. The calculation of the magnetization of a particle is explained in Sec. 3. Different magnetization models from the literature are discussed. In Sec. 4 we derive an expression to evaluate the magnetization of the MRF in the simulation. In Sec. 5 we show first simulation results and bring them in comparison with experimental results from the literature.

2 DISCRETE ELEMENT MODEL

The numerical description of the MRF is based on the Discrete Element Method (DEM), originally proposed by Cundall and Strack to compute the motion of a large number of particles [7]. After the computation of the forces $\mathbf{F}_i$ on each particle, Newton's equation of motion

$$m_i^G \, \ddot{\mathbf{r}}_\mathbf{i} = \mathbf{F}_i \tag{1}$$

is solved numerically for an ensemble of particles $i = 1, \ldots, N$ with masses m_i^G and center of mass positions $\mathbf{r}_i$. We model the MRF clutch with a three-dimensional simulation box containing spherical particles, terminated by solid walls in one direction and with periodic boundary conditions in the other two directions.

The forces included in the model are magnetic interaction forces between the particles, elastic repulsion, and the Stokes' drag of the fluid on the particles. The wall is modeled as a dense and flat ensemble of non-magnetic particles. Gravity and Brownian forces are neglected.

2.1 Magnetic forces

The dipole-dipole interaction energy $E_{i,j}$ of two magnetic particles i and j with magnetic moments $\mathbf{m}_i$ and $\mathbf{m}_j$ is [8]

$$E_{i,j} = \frac{\mu_0}{4\pi} \left[\frac{\mathbf{m}_i \cdot \mathbf{m}_j}{r_{i,j}^3} - \frac{3}{r_{i,j}^5} \left(\mathbf{m}_i \cdot \mathbf{r}_{i,j}\right) \left(\mathbf{m}_j \cdot \mathbf{r}_{i,j}\right) \right], \tag{2}$$

where $\mathbf{r}_{i,j} = \mathbf{r}_i - \mathbf{r}_j$ is the vector connecting the centers of particle i and j, $r_{i,j} = |\mathbf{r}_{i,j}|$ its norm and $\mu_0 = 4\pi \cdot 10^{-7} \, \frac{\mathrm{Tm}}{\mathrm{A}}$ the vacuum permeability.

The force on dipole i caused by dipole j is given by

$$\begin{aligned} \mathbf{F}_{i,j} &= -\boldsymbol{\nabla}_i E_{i,j} \\ &= \frac{3\mu_0}{4\pi} \left[\frac{\left(\mathbf{m}_i \cdot \mathbf{m}_j\right) \mathbf{r}_{i,j} + \left(\mathbf{m}_j \cdot \mathbf{r}_{i,j}\right) \mathbf{m}_i + \left(\mathbf{m}_i \cdot \mathbf{r}_{i,j}\right) \mathbf{m}_j}{r_{i,j}^5} - 5 \frac{\left(\mathbf{m}_i \cdot \mathbf{r}_{i,j}\right) \left(\mathbf{m}_j \cdot \mathbf{r}_{i,j}\right) \mathbf{r}_{i,j}}{r_{i,j}^7} \right]. \end{aligned} \tag{3}$$

The total magnetic force on particle i is then the sum of the contributions of all other particles j

$$\mathbf{F}_{\mathrm{i}} = \sum_{\substack{j \\ j \neq i}} \mathbf{F}_{i,j}. \tag{4}$$

The magnetic moments of the particles depend on the local magnetic field. The dependence is specified by a magnetization function which is described in detail in Sec. 3.2.

2.2 Hydrodynamic forces

The fluid acts on the particles via Stokes' drag,

$$\mathbf{F}_i^{\mathrm{Stokes}} = 6\pi\eta R_i \left(\mathbf{v}_{\mathrm{fluid}} - \mathbf{v}_i\right), \tag{5}$$

where $\mathbf{v}_i$ is the velocity of particle i, R_i is the particle radius, $\mathbf{v}_{\mathrm{fluid}}$ is the velocity of the carrier oil and η its viscosity.

2.3 Contact forces

A repulsive contact force which prevents the particles from overlapping is included. The normal force of particle j on particle i is given by the Hertzian repulsion

$$\mathbf{F}_i^{\mathrm{n}} = \left(\frac{\frac{2}{3}Y}{1-\nu^2} \sqrt{\frac{R_i R_j}{R_i + R_j}} \xi_{i,j}^{3/2} \right) \frac{\mathbf{r}_{i,j}}{r_{i,j}} \ , \tag{6}$$

where Y is Young's modulus, ν is Poissons's ratio, and $\xi_{i,j} = \max\{R_i + R_j - |\mathbf{r}_{i,j}|, 0\}$ the overlap [9].

As a first approach, no tangential forces are assumed.

3 TREATMENT OF THE MAGNETIC INTERACTIONS

In this section we introduce a selfconsistent algorithm for the calculation of the local magnetic field as well as general features of the single-particle magnetization function (Sec. 3.1). Three specific magnetization models are then discussed in Sec. 3.2.

3.1 Selfconsistent calculation of local magnetic induction and particle magnetization

The local magnetic induction at the position of particle i,

$$\mathbf{B}_{i,\mathrm{ext}} = \mathbf{B}_{\mathrm{applied}} + \sum_{\substack{j \\ j \neq i}} \mathbf{B}_{i,j} \ , \tag{7}$$

is given by the sum of the externally applied magnetic field $\mathbf{B}_{\mathrm{applied}} = \mu_0 \mathbf{H}_{\mathrm{applied}}$ and the sum of the contributions from other particles

$$\mathbf{B}_{i,j} = \frac{\mu_0}{4\pi}\left[3\frac{(\mathbf{m}_j \cdot \mathbf{r}_{i,j})\,\mathbf{r}_{i,j}}{r_{i,j}^5} - \frac{\mathbf{m}_j}{r_{i,j}^3}\right]. \tag{8}$$

The magnetization $\mathbf{M}_i$ of particle i is $\mathbf{M}_i = \frac{\mathbf{m}_i}{V_i}$ where V_i is the volume of particle i. The magnetic field $\mathbf{H}_{i,\text{in}}$ at the interior of particle i is given by [3]

$$\mathbf{H}_{i,\text{in}} = \frac{1}{\mu_0}\mathbf{B}_{i,\text{ext}} + \alpha\mathbf{M}_i. \tag{9}$$

The parameter α thus describes the contribution of the particle's own magnetization to its inner field $H_{i,\text{in}}$.

For the magnetization of the particle, we consider a model of the form

$$\mathbf{M}_i = |\mathbf{M}_S| f(b|\mathbf{H}_{i,\text{in}}|)\frac{\mathbf{B}_{i,\text{ext}}}{B_{i,\text{ext}}}\ , \tag{10}$$

where $\mathbf{M}_S$ is the saturation magnetization of the particle and f is a scaled magnetization function which is linear for small $|\mathbf{H}_{i,\text{in}}|$ and tends to 1 for large $|\mathbf{H}_{i,\text{in}}|$. The parameter b is chosen such that the slope for small fields matches the low-field susceptibility χ of the material.

As $\mathbf{H}_{\text{in}}$ itself depends on $\mathbf{M}$, Eq. (10) is an implicit equation. We solve this equation numerically by a root-finding algorithm that combines Newton-Raphson with the bisection method for a fail-safe routine [10]. We approach the solution of the coupled equations (7), (8) and (10) by the following iterative algorithm.

1. Initial step: $\mathbf{M}_i = 0$, $\mathbf{B}_{\text{i,ext}} = \mathbf{B}_{\text{applied}}$
2. Solve Eq. (10) with root-finding algorithm, update $\mathbf{M}_i$ for all i
3. Update $\mathbf{B}_{\text{i,ext}}$ for all i with equations (7) and (8)
4. Repeat steps 2. and 3. until the convergence criterion

$$\max_i |\mathbf{M}_i(n) - \mathbf{M}_i(n-1)| < \epsilon \tag{11}$$

is reached, where $\mathbf{M}_i(n)$ is the magnetization of particle i in the n-th iteration.

The positions of the particles are not changed during the selfconsistency loop.

3.2 Different magnetization models proposed in the literature

Magnetorheological fluids are mostly suspensions of carbonyl iron powder, a highly pure iron, where magnetic hysteresis is negligible [4]. Therefore we consider only models of the form of Eq. (10), describing anhysteretic magnetization behaviour. In this section three different choices for the magnetization function f as introduced in Eq. (10) are presented, the role of the model parameters is discussed, and the different models are compared.

3.2.1 Three magnetization functions

The three models we want to compare are the following:

1. A simple magnetization function for axially anisotropic materials with applied field along the easy axis, found in [2]

$$\mu_0 M = \mu_0 M_S \tanh(\frac{\chi}{M_S} H_{\text{in}}) \tag{12}$$

2. A phenomenological model for isotropic materials, based on the modified Langevin function [3]

$$\mu_0 M = \mu_0 M_S \left(\coth(\frac{3\chi}{M_S} H_{\text{in}}) - \frac{1}{\frac{3\chi}{M_S} H_{\text{in}}} \right) \tag{13}$$

3. The Fröhlich-Kennely law for the magnetization of a particle located inside an infinite chain [4]

$$\mu_0 M = \mu_0 M_S \, \frac{\frac{\chi}{M_S} H_{\text{in}}}{1 + \frac{\chi}{M_S} H_{\text{in}}} \tag{14}$$

3.2.2 How to choose the parameters

Saturation magnetization M_S is the saturation magnetization of the material of the spheres. This value can be obtained experimentally. Following [11], the saturation magnetization M_S of the suspension of particles and carrier oil can be related to the saturation magnetization of the bulk magnetic solid $M_{S,\text{bulk}}$ by the volume fraction ϕ of the suspension, $M_S = \phi M_{S,\text{bulk}}$.

Susceptibility and α All chosen models are constructed in a way that

$$M \sim \chi H_{\text{in}} \text{ for small } H_{\text{in}}, \tag{15}$$

where $\chi = \chi_{\text{mat}}$ is the susceptibility of the material. The susceptibility χ_{part} of a particle is given by

$$M \sim \chi_{\text{part}} H_{\text{ext}} \text{ for small } H_{\text{ext}}. \tag{16}$$

Combining equations (9), (15) and (16), we get

$$\chi_{\text{mat}} = \frac{\chi_{\text{part}}}{1 + \alpha \chi_{\text{part}}}. \tag{17}$$

Unfortunately, the single particle parameters are usually not known. In experiments, the magnetization curve of the whole MRF is measured instead [12]. Thus we have to infer

the susceptibility of the particle from the experimentally measured magnetization curve of the MRF.

Regarding the parameter α, one obtains for uniformly magnetized spheres $\alpha = -\frac{1}{3}$ and thus $\chi_{\text{sphere}} = \frac{3\chi_{\text{mat}}}{3+\chi_{\text{mat}}}$ [8]. In other cases, α is a coupling parameter depending on the coupling of the magnetic domains inside the particle and on the particle geometry and has to be fitted to experiments [3, 8].

3.2.3 Comparison of the magnetization models

Figure 1 shows the different magnetization models for parameter values $\mu_0 M_S = 1.709\,\text{T}$ (taken from [4]), $\alpha = -1/3$ (uniformly magnetized spheres) and a susceptibility $\chi_{\text{mat}} \approx 5.7$.

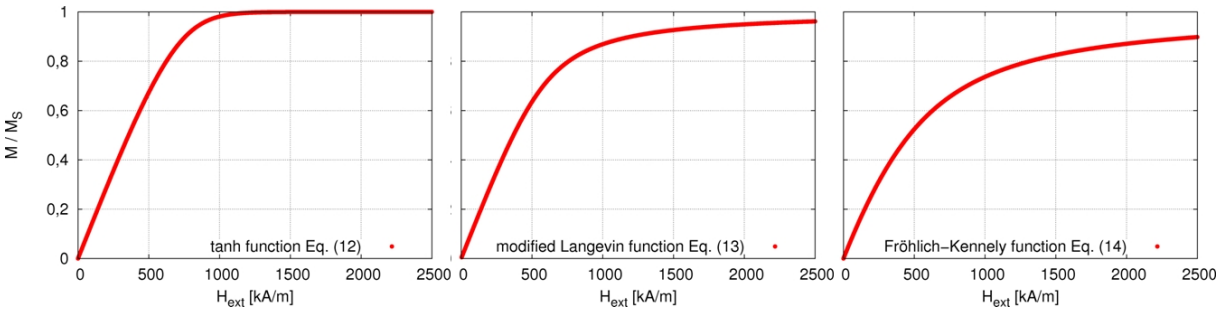

Figure 1: Comparison of the three magnetization functions Eq. (12), Eq. (13), and Eq. (14).

We see that the three models differ strongly in their behaviour for intermediate field strength. The tanh function is very steep and approaches saturation early. The modified Langevin function deviates from the linear regime for small fields earlier and needs stronger fields to reach saturation. The same holds for the Fröhlich-Kennely function, only that the effects are still more pronounced.

4 DEFINITION OF THE MRF MAGNETIZATION

Experimentally the magnetization of the MRF is obtained by

$$\mu_0 M = B_{\text{measured}} - \mu_0 H_{\text{applied}}, \tag{18}$$

where H_{applied} is the externally applied magnetic field, controlled by a electromagnet, and B_{measured} is the magnetic induction measured at a location close to the MRF.

If we want to mimic the experimental procedure in the simulation, we need to choose a point where to measure the magnetization. We can–similarly to the experiment–apply a certain external field H and measure the magnetic induction B at some point close to the MRF. Figure 2 shows the value of $B_{\text{measured}} - B_{\text{applied}}$ for a setup where the MRF is between two discs at $z = \pm 37.5\ \mu$m. B_{measured} is the measured magnetic induction in the simulation (at $y = 0$, averaged in x-direction) as a function of the measuring position,

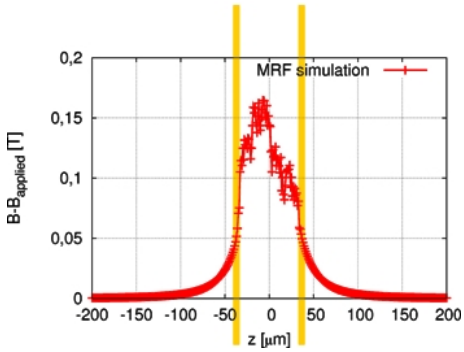

Figure 2: Locally measured magnetic induction (only the contribution of the MRF, without externally applied field). The MRF is located between the yellow bars.

called z_0, in z-direction. We see that the measured value depends significantly on the distance of the measuring point from the MRF. However, we want to have a value for the magnetization of the MRF, which is independent of the measuring point. To this purpose, we analyze the contribution of the MRF to the magnetic field B at distances far from the MRF. The behaviour of the absolute value of the magnetic field for large distances from

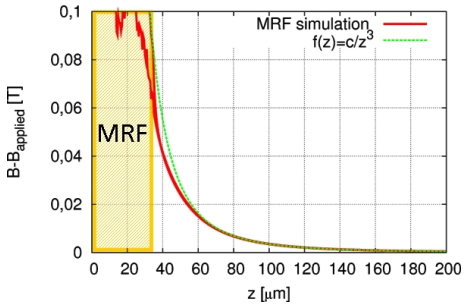

Figure 3: Magnetic field B induced by the MRF, far from the MRF.

the MRF can be described by

$$|B_{\text{measured}}(z) - B_{\text{applied}}| = \frac{c}{z^3} \tag{19}$$

with a constant c, as shown in Fig. 3. Thus the field of the MRF shows the same decay as a magnetic dipole field. We therefore define the magnetic moment of the MRF $\mathbf{m}_{\text{MRF}}$ as the magnetic dipole moment inducing the same magnetic field B as the MRF at larger distances from the MRF.

A magnetic dipole located at the origin with dipole moment $\mathbf{m} = m\mathbf{e}_z$ creates a magnetic field

$$\mathbf{B}_{\text{dipole}}(z) = \frac{\mu_0}{2\pi} \frac{\mathbf{m}}{|z|^3} \tag{20}$$

at location $(0, 0, z)$. The value of $m_{\mathrm{MRF}} = |\mathbf{m}_{\mathrm{MRF}}|$ can be found by fitting the large-distance magnetic field B (19), yielding

$$m_{\mathrm{MRF}} = c\ \frac{2\pi}{\mu_0}. \tag{21}$$

Another expression for the MRF magnetization can be obtained by considering that, seen from a larger distance from the MRF, the magnetic dipoles carried by the particles inside the MRF are approximately at the same spot. With the superposition principle we get for the field created by the MRF:

$$\mathbf{B}_{\mathrm{MRF}}(z) = \sum_i \mathbf{B}_i(z) = \sum_i \frac{\mu_0}{2\pi}\ \frac{\mathbf{m}_i}{|z|^3} = \frac{\mu_0}{2\pi}\ \frac{1}{|z|^3} \sum_i \mathbf{m}_i\ , \tag{22}$$

where $\mathbf{B}_i$ is the magnetic field created by particle i and $\mathbf{m}_i$ is the magnetic moment of particle i. On the other hand

$$\mathbf{B}_{\mathrm{MRF}}(z) = \frac{\mu_0}{2\pi}\ \frac{\mathbf{m}_{\mathrm{MRF}}}{|z|^3}. \tag{23}$$

Combining the equations (22) and (23) we get

$$m_{\mathrm{MRF}} = \left| \sum_i m_i \right|. \tag{24}$$

Thus, we expect the two definitions (21) and (24) for m_{MRF} to be equivalent. To test this hypothesis, we performed simulations with an externally applied field of $\mu_0 H = 0.14$ T, 0.42 T, and 1.4 T. The results are shown in Table 1.

Table 1: Comparison of the two definitions for the magnetic moment of the MRF.

$\mu_0 H_{\mathrm{applied}}$ [T]	0.14	0.42	1.4
$m = c\ \frac{2\pi}{\mu_0}$ [Am^2]	2.40×10^{-8}	5.94×10^{-8}	6.92×10^{-8}
$m = \sum_i m_i$ [Am^2]	2.38×10^{-8}	5.90×10^{-8}	6.86×10^{-8}

The differences between the definitions amount to less than 1 % of the magnitude of the magnetic moment. Therefore the two definitions can be regarded as equivalent. For our simulations, we take $\mathbf{m}_{\mathrm{MRF}} = \sum_i \mathbf{m}_i$ as the working definition. $\mathbf{M}_{\mathrm{MRF}}$ is then defined as

$$\mathbf{M}_{\mathrm{MRF}} \quad = \quad \frac{\mathbf{m}_{\mathrm{MRF}}}{V_{\mathrm{MRF}}} = \frac{N\ \langle \mathbf{m}_{\mathrm{part}} \rangle}{V_{\mathrm{MRF}}} = \phi\ \langle \mathbf{M}_{\mathrm{part}} \rangle. \tag{25}$$

The MRF magnetization for monodisperse suspensions can thus be expressed as the average particle magnetization $\langle \mathbf{M}_{\text{part}} \rangle = \frac{\langle \mathbf{m}_{\text{part}} \rangle}{V_{\text{part}}}$ times the volume fraction $\phi = \frac{N\, V_{\text{part}}}{V_{\text{MRF}}}$, where V_{part} is the volume of one particle, V_{MRF} the volume of the MRF, and N the number of particles in the MRF.

Equation (25) provides a convenient definition for the magnetization of the MRF in the simulation. The experimentally measured magnetization however still depends on the unknown measuring point. We can get independence from the measuring point by dividing the measured magnetization by the measured high-field saturation value at the same measuring point. This gives transformed experimental values

$$\frac{|B(z_0) - B_{\text{applied}}|}{|B_S(z_0) - B_{\text{applied}}|} = \frac{\frac{\mu_0}{2\pi} \frac{m^{\text{exp}}_{\text{MRF}}}{|z_0|^3}}{\frac{\mu_0}{2\pi} \frac{m^{\text{exp}}_{\text{S,MRF}}}{|z_0|^3}} = \frac{m^{\text{exp}}_{\text{MRF}}}{m^{\text{exp}}_{\text{S,MRF}}} \tag{26}$$

The same can be done for the computed magnetization

$$\frac{M_{\text{MRF}}}{M_{\text{S,MRF}}} = \frac{m_{\text{MRF}}}{m_{\text{S,MRF}}} \tag{27}$$

With this scaling procedure, the experimental [Eq. (26)] and computed [Eq. (27)] magnetization values can be put in comparison.

5 RESULTS

Here we present DEM-simulation results at different volume fractions with spherical particles of 1 μm in diameter, comparable to the experiments reported in [4]. We used the tanh model with values from Sec. 3.2.3. In the simulations we see that the magnetization curve of the MRF deviates significantly from the single sphere curve (Fig. 4). Figure 5

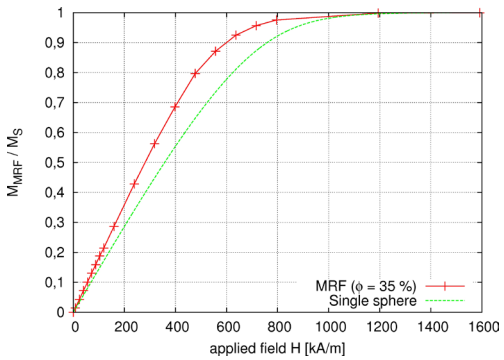

Figure 4: Scaled magnetization curve of the MRF ($\phi = 35$ %) compared with the single sphere curve.

shows the unscaled MRF magnetization curves simulated at different volume fractions ϕ. In Ref. [4], the relative differential permeability curves of MRF are shown instead of the

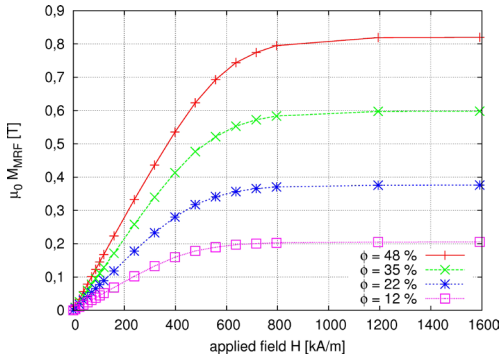

Figure 5: Magnetization curves of the MRF for different volume fractions ϕ.

magnetization. From simulations, we get the relative differential permeability $\mu_{\mathrm{r,dif}}$ of the MRF as

$$\mu_{\mathrm{r,dif}}(B) = 1 + \mu_0 \frac{dM_{\mathrm{MRF}}}{dB} \tag{28}$$

The simulation results are shown in Fig. 6. As stated in Sec. 3.2.2, we can get experimental

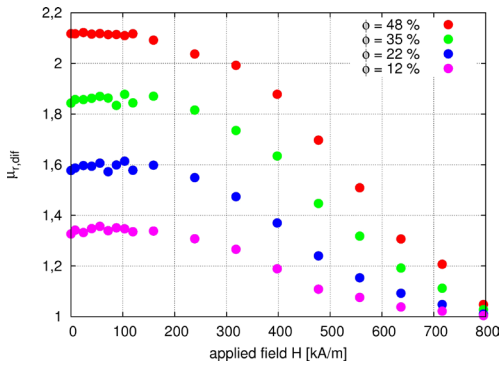

Figure 6: Relative differential permeability $\mu_{\mathrm{r,dif}}$ for different volume fractions ϕ of the MRF from DEM-simulations.

values for the low-field susceptibility χ_{MRF} of the MRF, whereas the susceptibility of the material χ_{mat} is unknown. The susceptibility χ_{MRF} is related to the relative differential permeability by

$$\chi_{\mathrm{MRF}} \quad = \quad \mu_{\mathrm{r,dif}}(0) - 1. \tag{29}$$

The computed values are shown in Fig. 7. The linear dependence of χ_{MRF} on volume fraction is also observed in experiments [4]. The susceptibility there is much higher though. By increasing the susceptibility of the material χ_{mat} we also get higher susceptibilities for the MRF (see figure 8). However, the exact dependence still has to be investigated.

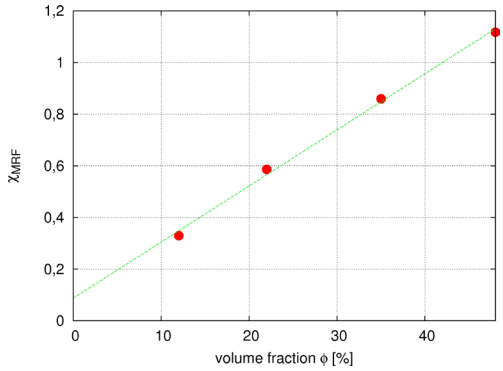

Figure 7: Low-field susceptibility of the MRF from DEM-simulations vs. volume fraction ϕ.

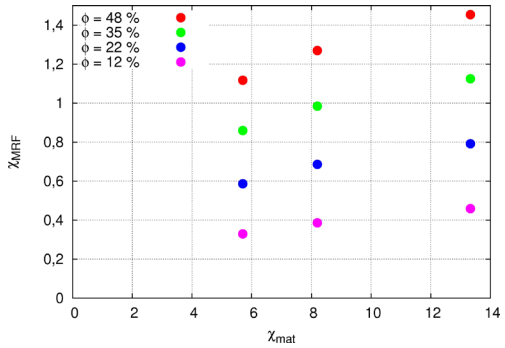

Figure 8: Low-field susceptibility of the MRF vs. material susceptibility χ_{mat} for different volume fractions ϕ.

6 CONCLUSIONS

A numerical model of a magnetorheological fluid based on the Discrete Element Method with emphasis on the magnetization model was presented. The magnetic interactions were treated using a selfconsistent algorithm. For the description of the anhysteretic magnetization curve of the particles, three magnetization models from the literature were compared. An expression for the magnetization of the MRF in the simulation was derived, thus enabling the comparison of experimental and computed magnetization curves.

From simulations we see that the magnetization curve of the MRF deviates significantly from the single sphere curve. The low-field susceptibility of the MRF depends linearly on volume fraction. The material's susceptibility, which is needed as a parameter for the magnetization model, can be obtained by comparing the resulting MRF susceptibility to experiments.

REFERENCES

[1] Furst E M and Gast A P, Phys. Rev. E **61**, 6732 (2000).

[2] Raghunathan A, Melikhov Y, Snyder J E, and Jiles D C, Appl. Phys. Lett. **95**, 172510 (2009).

[3] Jiles D C and Atherton D L, J. Magn. Magn. Mater. **61**, 48 (1986).

[4] de Vicente J, Bossis G, Lacis S, and Guyot M, J. Magn. Magn. Mater. **251**, 100 (2001).

[5] Jiles D C, Thoelke J B, and Devine M K, IEEE Trans. Magn. **28**, 27 (1992).

[6] Ehrlich J, Böse H, Private communication.

[7] Cundall P A and Strack O D L, Geotechnique **29**, 47 (1979)

[8] Jackson J D, *Classical Electrodynamics*. Wiley (1998).

[9] Hertz H, J. reine angew. Math. **92**, 156 (1881).

[10] Press W H, Teukolsky S A, Vetterling W T, and Flannery B P, *NUMERICAL RECIPES in Fortran 77*. Cambridge Univ. Press (1992).

[11] Rosensweig R E, *Ferrohydrodynamics*. Dover Publications (1997).

[12] Jolly M R, Carlson J D, and Muñoz B C, Smart Mater. Struct. **5**, 607 (1996).